

## An Estimation of the Star Formation Rate in the Perseus Complex

Seyma Mercimek<sup>1,2</sup>, Philip C. Myers<sup>1</sup>, Katherine I. Lee<sup>1</sup>, Sarah I. Sadavoy<sup>1</sup>

<sup>1</sup>*Harvard-Smithsonian Center for Astrophysics, 60 Garden Street, Cambridge, MA 02138, USA;*  
*smercimek@ogr.iu.edu.tr*

<sup>2</sup>*Istanbul University, Graduate School of Science and Engineering, Bozdogan Kemerli Cad. 8,*  
*Vezevceiler-Istanbul-Turkey*

### ABSTRACT

We present the results of our investigation of the star-forming potential in the Perseus star forming complex. We build on previous starless core, protostellar core, and young stellar object (YSO) catalogs from *Spitzer* (3.6-70  $\mu\text{m}$ ), *Herschel* (70-500  $\mu\text{m}$ ), and SCUBA (850  $\mu\text{m}$ ) observations in the literature. We place the cores and YSOs within seven star-forming clumps based on column densities greater than  $5 \times 10^{21} \text{ cm}^{-2}$ . We calculate the mean density and free-fall time for 69 starless cores as  $\sim 5.55 \times 10^{-19} \text{ g cm}^{-3}$  and  $\sim 0.1 \text{ Myr}$ , respectively, and we estimate the star formation rate for the near future as  $\sim 150 M_{\odot} \text{ Myr}^{-1}$ . According to Bonnor-Ebert stability analysis, we find that majority of starless cores in Perseus are unstable. Broadly, these cores can collapse to form the next generation of stars. We found a relation between starless cores and YSOs, where the numbers of young protostars (Class 0 + Class I) are similar to the numbers of starless cores. This similarity, which shows a one-to-one relation, suggests that these starless cores may form the next generation of stars with approximately the same formation rate as the current generation, as identified by the Class 0 and Class I protostars. It follows that if such a relation between starless core and any YSO stage exists, SFR values of these two populations must be nearly constant. In brief, we propose that this one-to-one relation is an important factor in better understanding the star formation process within a cloud.

*Subject headings:* ISM: individual objects (Perseus) — stars: formation — stars: protostars

### 1. Introduction

The Perseus molecular cloud is an excellent region to study dense cores and young stellar objects (YSOs) in terms of intermediate and low-mass star formation within isolated and clustered

conditions (Bally et al. 2008, p. 308). Perseus is relatively nearby at 235 pc (Hirota et al. 2011), and many studies have already investigated its dense core and YSO populations using continuum observations (e.g., Enoch et al. 2006; Kirk et al. 2006; Evans et al. 2009; Young et al. 2015) and molecular line emission (e.g., Hatchell et al. 2005; Rosolowsky et al. 2008; Foster et al. 2009) from different telescopes. In particular, studies have used these population surveys to classify dense cores as protostellar or starless (e.g., Enoch et al. 2008; Jørgensen et al. 2008; Sadavoy et al. 2010).

In addition to studying populations of dense cores and YSOs, continuum observations can also reveal different cloud structures on larger scales. Molecular clouds have a lot of structure, whereas the dense cores and YSOs are often embedded in filaments (e.g., André et al. 2010) or in moderately dense, larger-scale ( $\sim 1$  pc) clumps (see Di Francesco et al. 2007, p. 17). Column density (or extinction) maps from continuum observations of entire clouds are excellent tools to trace these structures (e.g., Schneider et al. 2015), and several studies have produced such maps for Perseus (e.g., Ridge et al. 2006; Sadavoy et al. 2014; Zari et al. 2016).

Connecting cores to their clumps is important, as cores represent the next generation of stars, and clumps represent the immediate star-forming potential. In this study, we primarily focus on the starless cores and exclude protostellar cores from our main analysis. Thus, we can estimate the next generation star formation rate (SFR) by counting the numbers of starless cores.

Many previous studies have measured SFRs of entire clouds based on their YSO populations, e.g.,  $57 M_{\odot} \text{ Myr}^{-1}$  in Serpens (Harvey et al. 2007),  $6.5 M_{\odot} \text{ Myr}^{-1}$  in Cha II (Alcalá et al. 2008), and  $73 M_{\odot} \text{ Myr}^{-1}$  in Ophiuchus (Evans et al. 2009). Evans et al. (2009) also found an SFR of  $96 M_{\odot} \text{ Myr}^{-1}$  for Perseus, which is relatively high compared to similar nearby clouds.

These previous studies generally used different number counts and considered different stages of YSOs. For example, Evans et al. (2009) determined SFRs by taking a mean mass of  $0.5 M_{\odot}$  in 2 Myr, which is the typical age of Class II sources. They included all YSO stages for the estimation. We choose a different way to estimate SFR in this study. Working on relations between numbers of YSOs stages and starless cores from clump to clump, we estimate SFR without including the all of the stages. In brief, we do not need to estimate lifetimes and masses of YSOs of all stages.

We describe the core and YSO catalogs in Section 2. We discuss the structures of clumps in Section 3. In Section 4, we present our analysis. Finally, we discuss our results and previous studies in Section 5.

## 2. Data

We used published catalogs of cores and YSOs at different wavelengths ranging from sub-millimeter ( $850 \mu\text{m}$ ) to the infrared ( $1.25 \mu\text{m}$ ). In the following section, we explain which data we used for the starless cores, the protostellar cores, and the YSOs.

## 2.1. Starless Cores and Protostellar Cores

Cores within molecular clouds can be observed in emission at wavelengths  $\gtrsim 100 \mu\text{m}$ , as these structures are generally cold ( $\lesssim 20 \text{ K}$ ), small ( $\lesssim 0.1 \text{ pc}$ ), and dense ( $\gtrsim 1 \times 10^5 \text{ cm}^{-3}$ ; Di Francesco et al. 2007, p. 17). Cores that have already contain protostars are identified from the presence of an internal heating source. For example Dunham et al. (2008), Evans et al. (2009), and Könyves et al. (2015) identified protostellar cores via compact  $70 \mu\text{m}$  emission. Several recent studies identified dense cores and classified them as protostellar or starless using infrared observations of protostars.

First, Jørgensen et al. (2008) combined observations from the *Spitzer* c2d survey and SCUBA/JCMT submillimeter data. This study classified cores as protostellar if there was an MIPS source located within  $15''$  of the core center. Second, Enoch et al. (2008) combined *Spitzer* c2d data with Bolocam millimeter observations for their sample. They identified protostellar cores using various infrared characteristics such as flux density, infrared colors, and proximities to the core center. Finally, Sadavoy et al. (2010) similarly used SCUBA and c2d data to classify cores in five clouds. Their classification scheme identified protostellar cores based on *Spitzer* YSOs within a flux-defined boundary, instead of using a fixed circular distance or the core sizes from previous classification studies. For this study, we adopt the core classifications from Sadavoy et al. (2010).

It is obvious that the number of cores between the three methods should be different, as each method focused on different criteria in order to classify cores as protostellar or starless. However, these numbers vary only slightly between the methods, as is shown in Table 1.

Table 1: Numbers of Starless Cores and Protostellar Cores in Perseus from the literature

Method	Starless Core	Protostellar Core
Sadavoy	97	46
Enoch	94	49
Jørgensen	101	42

## 2.2. Class 0 Sources

Class 0 sources are the youngest phase of YSOs, when most of the mass is contained within the dense core (Andre et al. 1993). As these sources are deeply embedded, they are detected at wavelengths from mid-IR to submillimeter (etc., Enoch et al. 2009, Sadavoy et al. 2014). In short, Enoch et al. (2009) combined Bolocam 1.1 mm and *Spitzer* c2d survey data. Sadavoy et al. (2014) identified Class 0 sources more comprehensively from clump to clump, combining *Herschel* data at  $70\text{-}500 \mu\text{m}$  and SCUBA data at  $850 \mu\text{m}$  with the c2d survey. These two studies also selected different criteria to identify Class 0 sources. Sadavoy et al. (2014) used the ratio of submillimeter to bolometric luminosity  $L_{\text{submm}}/L_{\text{bol}} \gtrsim 1\%$  (Andre et al. 2000, p. 59) whereas Enoch et al. (2009) used  $L_{\text{submm}}/L_{\text{bol}} \gtrsim 0.5\%$  (Andre et al. 1993). Consequently, Sadavoy et al. (2014) did not include

the extra four sources using  $L_{submm}/L_{bol} < 1\%$  in order to avoid taking borderline sources. In addition, they marked whether Class 0 sources were identified as a *Spitzer* sources. Thus, we can exclude late stage YSOs (in Section 3.2), which are overlapped with Class 0 sources using this indication (see also their list, Sadavoy et al. 2014). Although the numbers in two methods are the same (27/28), the sources are different. Accordingly, we used the Class 0 source list for Perseus from Sadavoy et al. (2014).

### 2.3. Young Stellar Objects (Class I to Class III)

We used *Spitzer* c2d data from Evans et al. (2009) to identify the later stages of YSOs. They identified sources as Class I-Flat-II-III using the updated classifications by Greene et al. (1994) (see also, Lada 1987, André et al. 1993, where sources were identified by their infrared spectral indices,  $\alpha$ , which measures the SED slope between  $\sim 2 - 24 \mu\text{m}$ ). The different classes are defined by:

**0/I**  $0.3 \leq \alpha$

**Flat**  $-0.3 \leq \alpha < 0.3$

**II**  $-1.6 \leq \alpha < -0.3$

**III**  $\alpha < -1.6$

We adopt the infrared spectral indices given in Evans et al. (2009) and correct for extinction in order to identify the quantity of these YSOs in Perseus. In addition, those sources identified as Class 0 from Sadavoy et al. (2014) were removed from the Class I list.

## 3. Results

### 3.1. Borders of Clumps and Sources in Clumps

We focus on seven clumps in Perseus, which Sadavoy et al. (2014) showed in their Figure 1. They defined these clumps and their boundaries using a fitted *Herschel*-derived column density map. The column density threshold of  $A_V \simeq 7$  mag is proposed as a star formation threshold by André et al. (2010), Lada et al. (2010), and Evans et al. (2014) and is equal to  $N(H_2) \sim 5 \times 10^{21} \text{cm}^{-2}$  (see also, Kirk et al. 2006; André et al. 2010). The contours of the clumps are based on these thresholds. The names of the clumps are B5, IC 348, B1-E, B1, NGC 1333, L1455, and L1448. We use the same column density threshold of  $N(H_2) \sim 5 \times 10^{21} \text{cm}^{-2}$  ( $A_V \simeq 7$  mag) for the clumps in Figure 1, which shows a  $350 \mu\text{m}$  map of Perseus from the *Herschel* Gould Belt Survey (André et

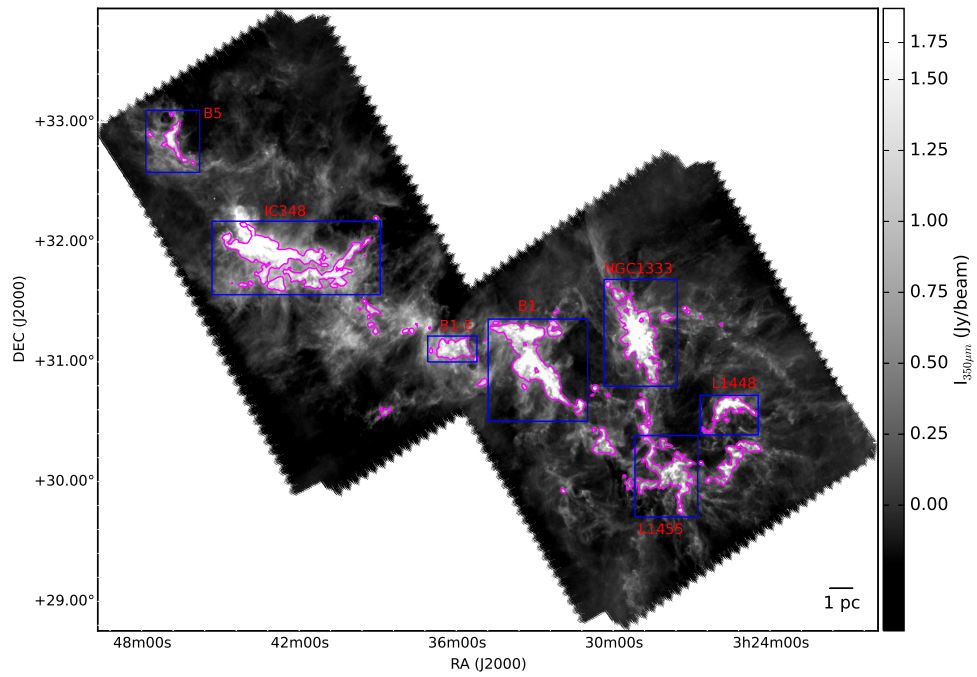


Fig. 1.— *Herschel* Level 2.5 image at 350  $\mu\text{m}$  of Perseus from the *Herschel* Science Archive. This map corresponds to pipeline-processed data with SPG v9.1.0. The contours are based on  $N(H_2) \sim 5 \times 10^{21} \text{ cm}^{-2}$ . The blue boxes are distinguish each clump from its neighbors.

al. 2010). Each Perseus clump is illustrated by purple contours, with its name appearing next to it. We exclude sources that are located outside of the clumps in this work.

We also list protostellar and starless cores in each clump, which is mentioned in Section 2.1. Table 2 gives the number of cores.

### 3.2. Clump

We considered a core or YSO to be associated with a clump if it is located within the  $A_V = 7$  mag contour of that clump from Sadavoy et al. (2014) (see also their Figure 1). We define a "source" to be a starless core or a YSO. Table 3 lists the quantity of each source in the seven clumps considered in this study. We did not count protostellar cores as sources, because these cores are SCUBA sources that coincided with a *Spitzer*-identified as Class 0/I/Flat YSO. Consequently, they would have been double-counted if added to the sources in Table 3. Thus, we only consider the starless cores for this study.

Perseus contains relatively more later-stage YSOs (Class II/III) than young protostars (Class 0/I), as is seen in other studies (e.g., Evans et al. 2009, Dunham et al. 2015). In addition, most of the sources are found in NGC 1333 and IC 348, which also show high surface densities of sources when compared to the other clumps. Conversely, B1-E and B5 have very few sources despite having  $\geq 50 M_\odot$  of material above the column density threshold of star formation.

Table 2: Number of Starless Cores and Protostellar Cores in Each Clump

Name of Clump	Starless Core	Protostellar Core
B5	0	1
B1-E	0	0
L1448	1	3
L1455	3	4
IC 348	26	9
NGC 1333	24	18
B1	15	8
All	69	43

---

Note. — The values are based on a column density level of  $N(H_2) > 5 \times 10^{21} \text{cm}^{-2}$  and cores from Sadavoy et al. (2010).

#### 4. Analyses

Figure 2 compares clump masses, the numbers of sources, and surface densities for each of the seven clumps. We order these clumps by mass. In general, we see an increasing trend with respect to those qualities. The clump mass has the added benefit of showing the star formation potential, e.g., the material above  $5 \times 10^{21} \text{ cm}^{-2}$  (the column density threshold).

According to Lada et al. (2010), the number of YSOs in a cloud should trend with the mass of that cloud above a threshold of  $A_V \simeq 7$  mag. Thus, we can make a direct comparison between the Perseus clumps and this expectation. Looking at Table 3, the trend does lean in that direction, but not all clumps appear to follow it perfectly (e.g., IC 348 has more objects than B1, but B1 has more mass above the threshold).

Among all clumps, B1-E has the lowest values in the number of cores and YSOs, while NGC 1333 has the highest values in both. Both IC 348 and NGC 1333 have significant excesses of YSOs including high fractions of Class II and Class III sources compared to starless cores, which suggests they started forming stars early in Perseus compared to the other clumps.

For the source surface densities, B1 again deviates from this trend, as does L1455, where both seem to have a lower surface densities for their mass. As L1448 and L1455 have a similar number of sources (shown in the middle Figure 2), the lower surface density in L1455 could be attributed to more clustered sources within a larger area. Because our surface densities are averages over the entire clump area for material with  $A_V \geq 7$  mag, highly clustered YSO environments can have underestimated surface densities relative to the larger clumps.

The deviation in source numbers of B1 suggests that this clump has not yet reached its star-forming potential. Since B1 has such a large star formation potential compared to its source count, the lack of objects suggests it is still very early in its star formation process. This region has very few "evolved YSOs" (and no Class III sources, see Table 3), which is indicative of a young population compared to NGC 1333 and IC 348 (see also Bally et al. 2008, p. 308).

As indicated in Table 3, B1-E does not show star formation activity. As B1-E is likely very young, it may still need time to form populations of dense cores and protostars (e.g., Sadavoy et al. 2015).

These same increase trends between those properties of each clump show that both surface densities and number of sources with clump masses increase following the order. For example, there is a linear correlation with coefficient value of 0.7 between clump masses and surface densities from clump to clump. On the other hand, this value could be higher if the surface density of B1 was not as low, as is shown in Figure 2. In the cases of either the absence or high surface density of B1, the correlation is approximate 1, which is a statistically robust linear relation.

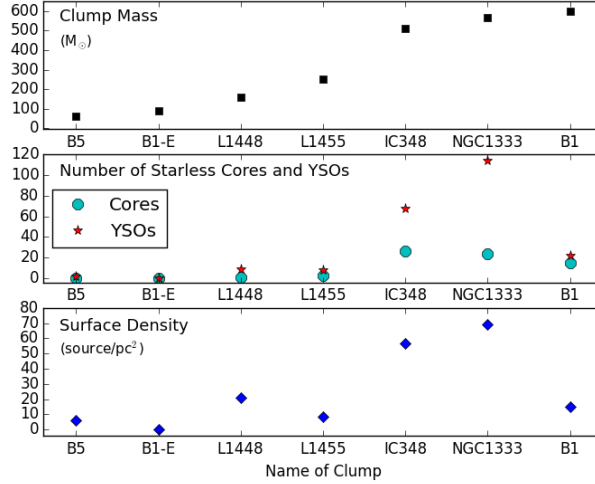


Fig. 2.— Comparison of clump mass (top), source counts (middle), and source surface density (bottom) for each clump in Perseus (see also Table 3).

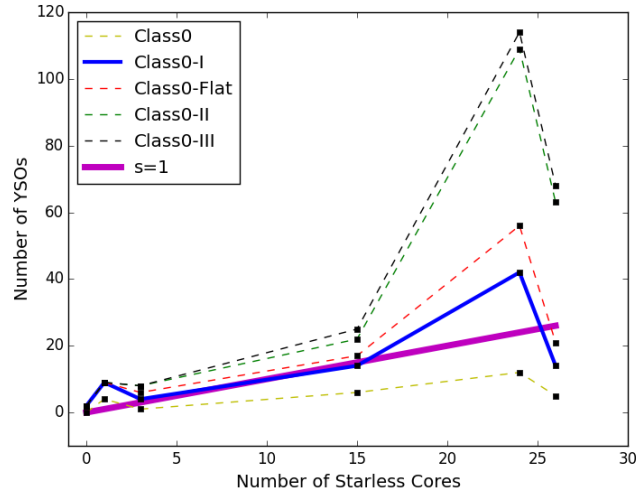


Fig. 3.— Number of starless cores vs. the number of YSOs for the Perseus clumps. From the bottom line to the top line, the order of the YSO classes is: Class 0, Class 0+I, Class 0+I+Flat, Class 0+I+Flat+II, and finally Class 0+I+Flat+II+III. The purple line illustrates a slope value of 1. This represents a one-to-one relation where the number of starless cores equals the number of YSOs. The blue line, Class 0+I, has the closest slope value to purple line. Clumps are shown by black squares and are ordered as B5, L1448, L1455, B1, NGC 1333, and IC 348, in order increasing number of starless core (not containing B1-E).



Table 3. Number of Sources in Each Clump

Name of Clump	Starless <sup>a</sup> Core	Class 0 <sup>b</sup>	Class I <sup>c</sup>	Class Flat <sup>c</sup>	Class II <sup>c</sup>	Class III <sup>c</sup>	Area <sup>b</sup> (pc <sup>2</sup> )	Surface Density (source pc <sup>-2</sup> )	Clump Mass <sup>b</sup> (M <sub>⊙</sub> )
B5	0	0	2	0	0	0	0.32	6.3	62
B1-E	0	0	0	0	0	0	0.57	0	88
L1448	1	4	5	0	0	0	0.48	20.8	159
L1455	3	1	3	2	2	0	1.3	8.5	251
IC 348	26	5	9	7	42	4	2.9	32	511
NGC 1333	24	12	30	14	53	5	2.0	69.0	568
B1	15	6	8	3	5	0	2.5	14.8	598
All	69	28	57	26	102	9	10.7	151.4	2237

Note. — The values are based on column density level of  $N(\text{H}_2) > 5 \times 10^{21} \text{ cm}^{-2}$ .

<sup>a</sup>From Sadavoy et al. (2010).

<sup>b</sup>From Sadavoy et al. (2014).

<sup>c</sup>YSO classes are determined from infrared spectral indices from Evans et al. (2009).

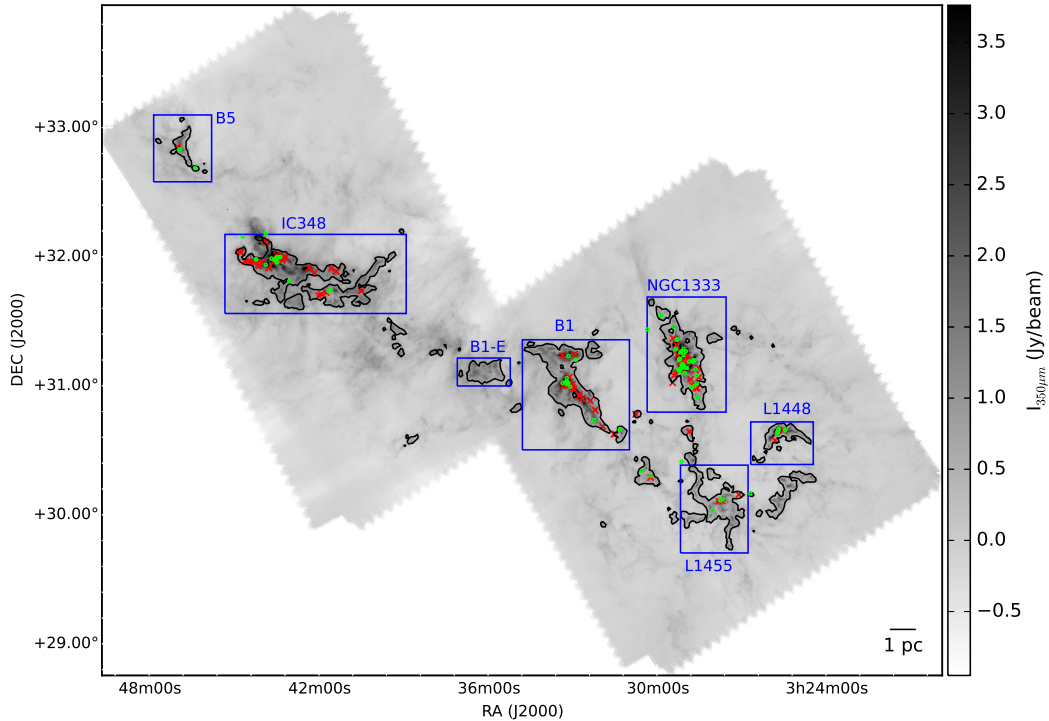


Fig. 4.— The seven Perseus clumps with their starless cores and Class 0+I protostars depicted here as red crosses and green circles, respectively. The background images are the same in Figure 1.

#### 4.1. Relationship Between Starless Cores and YSOs

Starless cores are the precursors to stars and represent the next generation of stars in molecular clouds. After they collapse, starless cores evolve into Class 0, Class I, Class Flat, Class II, and Class III, respectively. If starless cores reflect the star formation activity of the future, then the YSOs can be considered as the star formation activity of the recent past. By comparing these populations, we can determine how the star formation activity in Perseus is evolving.

Figure 3 compares the number of starless cores with the numbers of YSOs in each clump. We show distributions for cumulative YSO classifications starting from the youngest stage, Class 0. The thick, solid blue line shows the combined Class 0 and Class I source counts and has the best-fit slope of  $\sim 1.04$  (linear least square). This is similar to the purple line that illustrates a one-to-one relation between the starless cores and YSOs. Additionally, the correlation coefficient  $r$  between Class 0/I and starless cores is approximately 0.8, which indicates a strong linear relation. In other words, the starless cores appear to follow the number of young protostars (Class 0 + Class I) for all clumps in Perseus. In brief, we show with Figure 3 shows which YSO stage(s) are numerically similar to starless cores using values of their fit slopes.

Figure 4 shows starless cores and Class 0/I protostars in the each clump. The two populations show similar numbers and appear to follow the densest material in the cloud. More evolved YSOs may have moved from their original places of birth, as was recently suggested in Orion (Megeath et al. 2016, Stutz & Gould 2016). Because starless cores are considered the progenitors of stars, this similarity suggests that the SFR should be relatively similar between the current generation of young protostars and the next generation.

In order to examine that most of the starless cores in the Perseus clumps collapse, the Bonnor-Ebert mass of each core is estimated. If the Bonnor-Ebert sphere mass is less than the core mass, the starless core can collapse and form a new star (Spitzer 1968, p. 44). The critical mass values are defined by Ebert (1955) and Bonnor (1956):

$$M_{crit} = 1.18 \frac{c_s^4}{G^{3/2} P_{BE}^{1/2}}, \quad (1)$$

where  $c$  is the isothermal speed of sound.  $P_{BE} = \rho_o c_s^2$  is the boundary pressure of a core, where  $\rho_o$  is surface density of a core, assuming the core temperature is 10K. On the other hand, we can estimate the mean density of starless cores ( $\rho_{mean}$ ) with Equation 10. We calculated the Bonnor-Ebert sphere masses of the starless cores in Perseus (for the Bonnor-Ebert sphere, the ratio of mean density to surface density is 2.43).

Figure 5 shows the ratio of core masses to Bonnor-Ebert sphere masses. We know that if this ratio is greater than 1, cores are unstable and start collapsing, as mentioned above. Only 10 of the 69 starless cores (red column) have ratio less than 1. In the Bonnor-Ebert Model, all of the others (59 starless cores) are quite massive for stable equilibrium. We've also excluded three of the

most massive cores from the histogram, as their ratios exceeded 20. Even if we consider typical maximum mass with an uncertainty factor of 2 (the dotted line in Figure 5), we see substantial cores with masses greater than 2 times the Bonnor-Ebert masses. Dunham et al. (2016) worked on the stability of cores in Chameleon. Their study focused on whether starless cores in Chameleon are stable or not. According to their result, cores between 0.5 and 2 times the Bonnor-Ebert mass ( $0.5 M_{BE} < M < 2 M_{BE}$ ) are potentially unstable. While most of the cores in Chameleon are stable (core masses are under  $0.5 M_{BE}$ ), the majority of starless cores in Perseus are primarily unstable (core masses are above  $2 M_{BE}$ ). In the light of such information, we can assume that starless cores in Perseus collapse to make next generation of stars.

Assuming that the numbers of starless cores and protostars are equal, we estimate the future SFR.

$$\dot{M}_{stars,last} = \dot{M}_{stars,next} \quad (2)$$

where  $\dot{M}_{stars}$  is rate of stellar mass gain. Assuming steady state, we can eliminate times, resulting in,

$$M_{stars,last} = M_{stars,next}, \quad (3)$$

where  $M_{stars,last}$  and  $M_{stars,next}$  represent the masses of the protostars and the starless cores, respectively. Hereafter, we use  $M_{next}$  for  $M_{stars,next}$  and  $M_{last}$  for  $M_{stars,last}$ . Using Equation 5, the total mass of young protostars can be calculated, because we already have a value for the total mass of starless cores (from Sadavoy et al. 2010), which is  $\sim 190 M_{\odot}$  for 69 starless cores. Not all of the core mass goes into the next generation of stars. For instance, there is some efficiency factor (Alves et al. 2007) that must be considered. For the protostellar mass, Weidner & Kroupa (2006) estimated the average stellar mass for standard initial mass functions (IMFs) between 0.01 and  $150 M_{\odot}$  as,

$$\bar{m}_{IMF} = 0.36 M_{\odot}. \quad (4)$$

We assume that the average final masses of Class 0 and Class I YSOs are equal to  $\bar{m}_{IMF}$ , which means

$$M_{last} = N_{last} \bar{m}_{IMF}. \quad (5)$$

For 85 protostars, the expected mass of protostars is

$$M_{last} \cong 31 M_{\odot}. \quad (6)$$

With these numbers and masses of cores and stars, "core-star number efficiency" and "core-star mass efficiency" can be estimated as

$$\epsilon_{csn} = \frac{N_{last}}{N_{next}} \sim 1.2 \text{ and} \quad (7)$$

$$\epsilon_{csm} = \frac{M_{last}}{M_{next}} \sim 0.16. \quad (8)$$

Our analysis primarily assumes that all of our protostars are single systems. Nevertheless, many of the Perseus protostars are binaries or higher order multiples (see Lee et al. 2015, Tobin et al. 2016). If we were to consider multiple systems, then both  $\epsilon_{csm}$  and  $\epsilon_{csn}$  would increase. Therefore, our values should be taken as lower limits (within the assumptions of this study) to achieve steady state. Thus, we find that at least 1.2 stars will be produced from a core and that at least 16% of the core mass will be turned into stars.

#### 4.2. Calculation of Free-fall Time and Weighted Mean Lifetime

If a cloud mass exceeds its virial mass, it should become unstable and collapse unless there is another mechanism of support, such as turbulence or magnetic fields (Bodenheimer 2011, p. 68). Without additional support, the cores collapse under self-gravity in a free-fall time,

$$t_{ff} = \left(\frac{3\pi}{32G\rho}\right)^{1/2}, \quad (9)$$

where  $\rho$  is the mean core density. We estimate these densities from the effective radii and masses of the starless cores (from Sadavoy et al. 2010), assuming spherical symmetry. We find a mean starless core density

$$\bar{\rho} = 5.55 \times 10^{-19} \text{ g cm}^{-3}. \quad (10)$$

Figure 6 shows the distribution of free-fall times for all 69 starless cores, using Equation (9), and their average densities. We find a narrow distribution of free-fall times with an average of

$$\bar{t}_{ff} = 0.10 \text{ Myr}. \quad (11)$$

Thus, we expect the starless cores to collapse in  $\sim 0.10$  Myr, if they are all nearly virialized.

The starless cores will only collapse on a free-fall time if they are unstable. For example, high internal turbulence could delay their collapse by several free-fall times (e.g., Nakano 1998). Nevertheless, if the starless core and protostars are in a steady state, we can assume that the starless core lifetime equals the protostellar core lifetime. We can estimate the protostellar core lifetime by a weighted mean time ( $\bar{\tau}$ ),

$$\bar{\tau} = \omega_0\tau_0 + \omega_I\tau_I, \quad (12)$$

where  $\omega_0$  and  $\omega_I$  are correspond to the fraction of Class 0 and Class I protostars, respectively (e.g.,  $N_{Class0} / N_{Class0+ClassI}$  and  $N_{ClassI} / N_{Class0+ClassI}$ ) and  $\tau_0$  and  $\tau_1$  are the lifetimes of the Class 0 and Class I stages. We adopt the lifetimes from Evans et al. (2009), which were 0.10 Myr and 0.44 Myr for Class 0 and Class I YSOs, respectively. Thus, we find a weighted mean lifetime of the Perseus young protostars of

$$\bar{\tau} = 0.33 \text{ Myr}. \quad (13)$$

Accordingly, we can assume the starless cores will form the next generation of protostars in 0.33 Myr. In units of the free-fall time, we find,

$$\frac{\bar{\tau}_{next}}{\bar{\tau}_{ff}} = 3.3. \quad (14)$$

Thus, actual formation time is less efficient than pure free-fall time by a factor of  $\epsilon_{cst} = 3.3$ , assuming steady state.

As a result, the average starless core makes approximately 1.2 stars in 3.3 free-fall times.

### 4.3. The SFR in Perseus

The SFR corresponds to the star-forming mass as a function of lifetime. Similar to the weighted mean lifetime (Equation 13), we found the weighted mean inverse lifetime as,

$$\overline{\tau^{-1}} = \omega_0\tau_0^{-1} + \omega_I\tau_I^{-1}, \quad (15)$$

$$\overline{\tau^{-1}} = (0.21 \text{ Myr})^{-1}. \quad (16)$$

According to this, we estimate the SFR, using our number counts of protostars and their weighted lifetime. Following from Equation 6 and Equation 16, the weighted SFR is

$$\overline{SFR} = M_{stars} \overline{\tau^{-1}}, \quad (17)$$

$$\overline{SFR} \cong 150 M_{\odot} \text{ Myr}^{-1}. \quad (18)$$

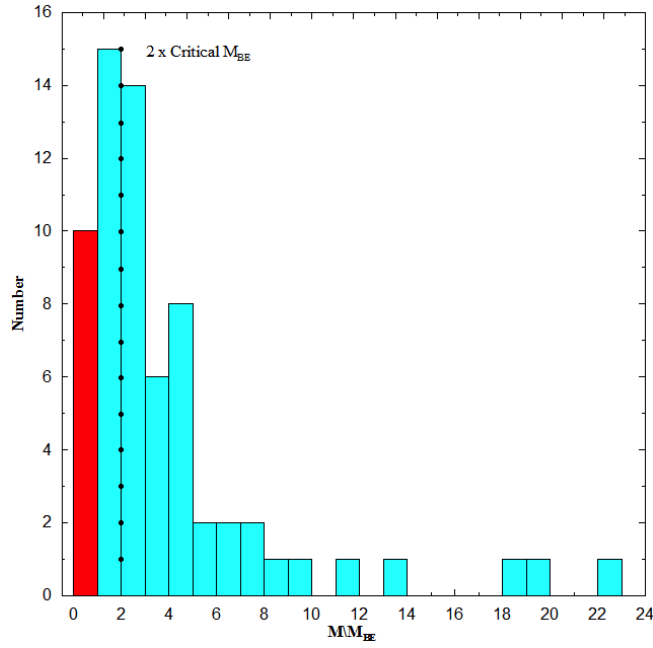


Fig. 5.— Histogram of the ratio of the starless core mass to the Bonnor-Ebert mass. Cyan columns depict ratios greater than 1, and the red column shows the ratios less than 1. The dotted line highlights  $2 \times M_{BE}$ .

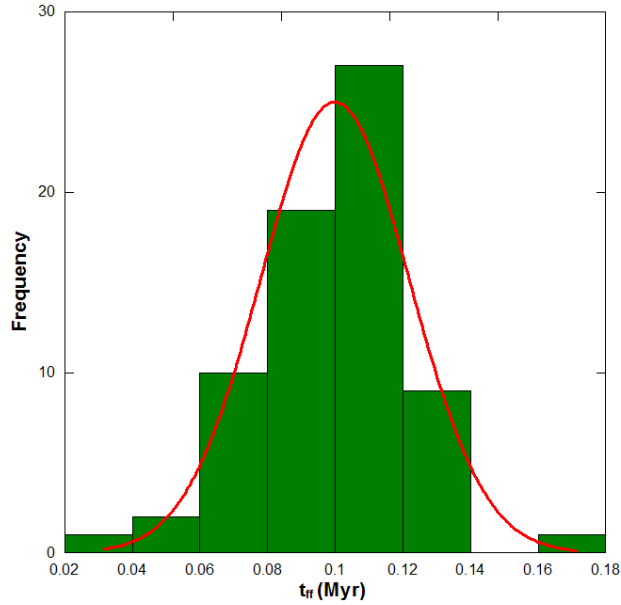


Fig. 6.— Histogram of the ratio of starless core free-fall times. The best-fit Gaussian has  $\mu, \sigma$  values of 0.10 Myr and 0.02 Myr, respectively.

## 5. Discussion

We estimated the SFR in Perseus using observations of young protostars and starless cores. We found that the SFR in Perseus is  $150 M_{\odot} \text{ Myr}^{-1}$  using  $M_{stars}$  and  $\bar{\tau}$ . If our SFR included close binary pairs, it could be higher. For example, if we instead take the starless cores, assuming 1.2 stars form per core at an efficiency of 16%, we get  $174 M_{\odot} \text{ Myr}^{-1}$ . In addition, 1.2 protostars from each core implies that there would be a binary fraction of 20% (one out of five cores will have a companion). The binary fraction from Tobin et al. (2016) is 40%, so the SFR could be a bit higher. Of course, the SFR values of clouds in the nearby Gould Belt are not as high as those in giant molecular clouds toward the Galactic plane, where high-mass stars are forming (e.g., Veneziani et al. 2013).

The SCUBA data used here will primarily pull out dense objects that are more likely to form stars in the near future. Following that, there is also the problem of starless core masses (single temperature, single dust properties, etc.); however, in the absence of robust temperature or more data, we cannot constrain these properties. With our assumptions (fixed dust temperatures and dust opacities for all starless cores, fixed stellar masses for the protostars, and a constant SFR between the protostars and the starless cores), our result  $\epsilon_{csm} = 0.16$  is similar to the value  $\epsilon_{csm} = 0.17$  found in Perseus by Jørgensen et al. (2008) using a similar method. These values are lower than the estimates  $\epsilon_{csm} = 0.3$  in the Pipe Nebula by Alves et al. (2007) and the  $\epsilon_{csm} = 0.4$  in Aquila by Könyves et al. (2015), by matching IMF with core mass functions. If we included multiple stellar systems or decreased the core mass (either by a higher dust temperature or a higher dust opacity),  $\epsilon_{csm}$  would increase. Therefore, the differences between our  $\epsilon_{csm}$  value and values of these studies could be due to these assumptions.

We found a near one-to-one relation between starless cores and protostars. This suggests that the SFR in Perseus may be constant (until the next generation) if all of the starless cores in this sample are likely to form stars in the near future. Because SCUBA observations are good at picking out the densest cores, whereas *Herschel* observations will also select more diffuse objects, it is reasonable to assume the SCUBA cores are likely to form new stars. According to Bonnor-Ebert criterion (Spitzer 1968, p. 44), core condition can be understood regardless of whether the core collapses to form new stars or not. If the ratio of the core mass to the critically Bonnor-Ebert sphere mass exceeds 1, then there is no equilibrium available, and the sphere is unstable against collapse. Subsequently, the core will collapse under its gravity. Assuming the core temperature is 10 K, nearly all (59 out of 69) starless cores are unstable in this work. Rates which go up to 142 are quite high. This means that core criteria (Sadavoy et al. 2010) with SCUBA observations tend to select dense cores.

We acknowledge that the main assumption of this study which states that a one-to-one relation can be used if most of starless cores in a cloud are unstable. Nevertheless, the majority of studies demonstrate that starless cores in a cloud are not unstable to collapse, using various methods to do so. For example, Belloche et al. (2011), Tsitali et al. (2015), and Dunham et al. (2016) found

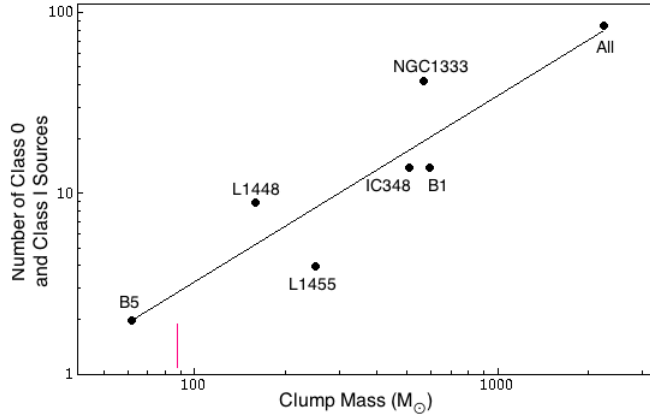


Fig. 7.— Number of protostars vs. clump masses. We show titled clumps with the included power-law tail (slope value of 1.08). The solid pink line shows where B1-E should be located.

that most of the starless cores in Cha I are stable, and cores cannot form stars. Following that, nearly all of the starless cores are stable in Orion B (Kirk et al. 2016). On the other hand, one recent study found that more than half of starless cores in the Aquila molecular cloud complex are unstable (Könyves et al. 2015). Considering all of these results, Perseus appears to be a special molecular cloud in terms of starless cores. Most of the starless cores in the cloud are unstable, and they will turn into stars in the near future.

We also compared the number of protostars with their clump properties. Figure 7 shows that the protostellar counts for the individual clumps (except B1-E because it has no sources) and the full Perseus cloud follow a power-law relation (slope value of 1.08) with clump mass similar to what Lada et al. (2010) found for entire clouds. We find more scatter than the Lada et al. (2010) relation, which considered YSOs of all stages. A similar plot of the clumps in Perseus is highly dependent on the population age. For example, both B1 and B1-E have relatively few sources of all stages given their clump masses (see Figure 2), and both are considered to be young regions. For individual clumps, it is possible that the population age plays a role, e.g., both B1 and B1-E have not had the chance to fully reach their star formation potential. Thus, in Figure 7, we consider just the young population (protostars), and the relation is quite good, even for B1 (excluding B1-E, which is still too young). The solid pink line in Figure 7 shows where B1-E should be located on this relation. We expect this clump to have about two protostars at the current epoch, whereas it has none.

This study shows that protostars and starless cores have nearly equal numbers in all seven clumps. Assuming the starless cores represent the next generation of stars and the Class 0/I sources represent the most recent generation of stars, the similarity between these two populations suggests a nearly constant SFR across each of the individual clumps in Perseus. In addition, we find a power-law relation between the number of protostars in individual clumps and the dense gas mass of those clumps (except B1-E). We also find that this relation scales with the total cloud



protostellar count and dense gas mass. Nevertheless, we do not see this same relation with clump mass when we also consider the more evolved YSOs. Using this approach, relations between sources and star formation can be used to study for other clouds.

This study was supported by research funding through AAG84 group (Üsküdar American Academy), which consists of benefactors who support successful female students in Turkey. We would like to thank to some group members who include Ayşın Akbarut, Zeynep Ataç, Filiz Diniz, Nil Canal, Zeynep Ece, Sara Angat, Ashihan Altinkaya, Neslihan Altinkaya, Günay Şen, Funda Cıbroğlu, Aysel Kartal, and Müge Tuna. We also thank to Dr. Michael M. Dunham (Harvard-Smithsonian Center for Astrophysics, Cambridge, USA) for useful suggestion and Prof. Yüksel Karataş (Istanbul University, Istanbul, Turkey) for his support during this work.

### A. Tables of Sources For Each Clump

We list cores and YSOs for each clump in the Perseus in Table 4 to Table 10. They are selected according to the contour of column density level as  $5 \times 10^{21} \text{cm}^{-2}$ . The ID field shows the number of sources in the clumps. The properties of starless cores and protostellar cores are obtained from Sadavoy et al. (2010) and one protostellar core in B5 from Kirk et al. (2006). We found the value of free-fall time using values in the Mass column and  $R_{eff}$  in Table 4. Class 0 sources and other YSOs are obtained from Sadavoy et al. (2014) and Evans et al. (2009), respectively.

### REFERENCES

- Alcalá, J. M., Spezzi, L., Chapman, N., et al. 2008, ApJ, 676, 427
- Alves, J., Lombardi, M., & Lada, C. J. 2007, A&A, 462, L17
- Andre, P., Ward-Thompson, D., & Barsony, M. 1993, ApJ, 406, 122
- Andre, P., Ward-Thompson, D., & Barsony, M. 2000, Protostars and Planets IV, 59
- André, P., Men'shchikov, A., Bontemps, S., et al. 2010, A&A, 518, L102
- Bally, J., Walawender, J., Johnstone, D., Kirk, H., & Goodman, A. 2008, Handbook of Star Forming Regions, Volume I, 4, 308
- Belloche, A., Parise, B., Schuller, F., et al. 2011, A&A, 535, A2
- Belikov, A. N., Kharchenko, N. V., Piskunov, A. E., Schilbach, E., & Scholz, R.-D. 2002, A&A, 387, 117

- Bodenheimer, P. H. 2011, *Principles of Star Formation: , Astronomy and Astrophysics Library*. ISBN 978-3-642-15062-3. Springer-Verlag Berlin Heidelberg, 2011, 68
- Bonnor, W. B. 1956, *MNRAS*, 116, 351
- Dunham, M. M., Crapsi, A., Evans, N. J., II, et al. 2008, *ApJS*, 179, 249-282
- Dunham, M. M., Allen, L. E., Evans, N. J., II, et al. 2015, *ApJS*, 220, 11
- Dunham, M. M., Offner, S. S. R., Pineda, J. E., et al. 2016, *ApJ*, 823, 160
- di Francesco, J., Evans, N. J., II, Caselli, P., et al. 2007, *Protostars and Planets V*, 17
- Di Francesco, J., Johnstone, D., Kirk, H., MacKenzie, T., & Ledwosinska, E. 2008, *ApJS*, 175, 277-295
- Ebert, R. 1955, *ZAp*, 37, 217
- Enoch, M. L., Young, K. E., Glenn, J., et al. 2006, *ApJ*, 638, 293
- Enoch, M. L., Evans, N. J., II, Sargent, A. I., et al. 2008, *ApJ*, 684, 1240
- Enoch, M. L., Evans, N. J., II, Sargent, A. I., & Glenn, J. 2009, *ApJ*, 692, 973-997
- Evans, N. J., II, Dunham, M. M., Jørgensen, J. K., et al. 2009, *ApJS*, 181, 321-350
- Evans, N. J., II, Heiderman, A., & Vutisalchavakul, N. 2014, *ApJ*, 782, 114
- Foster, J. B., Rosolowsky, E. W., Kauffmann, J., et al. 2009, *ApJ*, 696, 298
- Greene, T. P., Wilking, B. A., Andre, P., Young, E. T., & Lada, C. J. 1994, *ApJ*, 434, 614
- Harvey, P., Merín, B., Huard, T. L., et al. 2007, *ApJ*, 663, 1149
- Hatchell, J., Richer, J. S., Fuller, G. A., et al. 2005, *A&A*, 440, 151
- Hirota, T., Honma, M., Imai, H., et al. 2011, *PASJ*, 63, 1
- Jørgensen, J. K., Johnstone, D., Kirk, H., et al. 2008, *ApJ*, 683, 822
- Kainulainen, J., Beuther, H., Henning, T., & Plume, R. 2009, *A&A*, 508, L35
- Kirk, H., Johnstone, D., & Di Francesco, J. 2006, *ApJ*, 646, 1009
- Kirk, H., Di Francesco, J., Johnstone, D., et al. 2016, *ApJ*, 817, 167
- Könyves, V., André, P., Men'shchikov, A., et al. 2015, *A&A*, 584, A91
- Lada, C. J. 1987, *Star Forming Regions*, 115, 1

- Lada, C. J., Lombardi, M., & Alves, J. F. 2010, *ApJ*, 724, 687
- Lee, K. I., Dunham, M. M., Myers, P. C., et al. 2015, *ApJ*, 814, 114
- Megeath, S. T., Gutermuth, R., Muzerolle, J., et al. 2016, *AJ*, 151, 5
- Nakano, T. 1998, *ApJ*, 494, 587
- Nutter, D., & Ward-Thompson, D. 2007, *MNRAS*, 374, 1413
- Ridge, N. A., Di Francesco, J., Kirk, H., et al. 2006, *AJ*, 131, 2921
- Rosolowsky, E. W., Pineda, J. E., Foster, J. B., et al. 2008, *ApJS*, 175, 509
- Sadavoy, S. I., Di Francesco, J., André, P., et al. 2014, *ApJ*, 787, L18
- Sadavoy, S. I., Di Francesco, J., Bontemps, S., et al. 2010, *ApJ*, 710, 1247
- Sadavoy, S. I., Shirley, Y., Di Francesco, J., et al. 2015, *ApJ*, 806, 38
- Schneider, N., Ossenkopf, V., Csengeri, T., et al. 2015, *A&A*, 575, A79
- Spitzer, L., Jr. 1968, *Nebulae and Interstellar Matter*, 44
- Stutz, A. M., & Gould, A. 2016, *A&A*, 590, A2
- Tobin, J. J., Looney, L. W., Li, Z.-Y., et al. 2016, *ApJ*, 818, 73
- Tsitali, A. E., Belloche, A., Garrod, R. T., Parise, B., & Menten, K. M. 2015, *A&A*, 575, A27
- Ward-Thompson, D., & Whitworth, A. P. 2011, *An Introduction to Star Formation* by Derek Ward-Thompson and Anthony P. Whitworth. Cambridge University Press, 2011. ISBN: 9780521630306, 112
- Weidner, C., & Kroupa, P. 2006, *MNRAS*, 3
- Williams, J. P., & McKee, C. F. 1997, *ApJ*, 476, 166
- Veneziani, M., Elia, D., Noriega-Crespo, A., et al. 2013, *A&A*, 549, A130
- Young, K. E., Young, C. H., Lai, S.-P., Dunham, M. M., & Evans, N. J., II 2015, *AJ*, 150, 40
- Zari, E., Lombardi, M., Alves, J., Lada, C. J., & Bouy, H. 2016, *A&A*, 587, A106

Table 4. Starless Cores in Each Clump

ID	Name	R.A. (deg)	Decl. (deg)	Mass ( $M_{\odot}$ )	$R_{eff}$ (pc)
L1448					
1	J032525.4+304508	051.3558	+30.7522	1.164	2.8e-02
L1455					
1	J032703.2+301513	051.7633	+30.2536	1.421	4.1e-02
2	J032739.7+301211	051.9154	+30.2031	1.660	3.3e-02
3	J032746.6+301204	051.9442	+30.2011	1.558	3.4e-02
B1					
1	J033158.5+304700	052.9937	+30.7833	1.489	4.3e-02
2	J033217.6+304947	053.0733	+30.8297	7.223	5.5e-02
3	J033214.9+305435	053.0621	+30.9097	1.541	4.4e-02
4	J033243.5+305953	053.1812	+30.9981	4.810	6.9e-02
5	J033243.6+310002	053.1817	+31.0006	3.441	5.9e-02
6	J033249.7+310114	053.2071	+31.0206	0.394	2.4e-02
7	J033251.1+310156	053.2129	+31.0322	1.301	4.1e-02
8	J033301.8+310420	053.2575	+31.0722	6.590	7.5e-02
9	J033305.6+310502	053.2733	+31.0839	5.426	6.5e-02
10	J033305.1+310638	053.2712	+31.1106	1.592	4.3e-02
11	J033311.7+310956	053.2987	+31.1656	0.514	2.6e-02
12	J033318.2+310608	053.3258	+31.1022	1.352	3.9e-02
13	J033325.7+310543	053.3571	+31.0953	1.147	3.6e-02
14	J033301.0+312044	053.2542	+31.3456	2.140	5.0e-02
15	J033327.3+311955	053.3637	+31.3319	0.582	2.8e-02
IC 348					
1	J034146.4+315720	055.4433	+31.9556	0.753	3.1e-02
2	J034156.8+315844	055.4867	+31.9789	0.205	1.7e-02
3	J034234.5+315620	055.6437	+31.9389	0.462	2.5e-02
4	J034246.3+315837	055.6929	+31.9769	4.622	7.9e-02
5	J034338.3+320308	055.9096	+32.0522	2.020	4.2e-02
6	J034342.5+320320	055.9271	+32.0556	2.277	3.9e-02
7	J034344.0+320250	055.9333	+32.0472	2.876	4.2e-02
8	J034345.8+320138	055.9408	+32.0272	0.428	2.2e-02
9	J034347.7+320214	055.9487	+32.0372	0.770	2.9e-02
10	J034405.2+320045	056.0217	+32.0125	0.308	2.1e-02
11	J034414.4+315753	056.0600	+31.9647	1.660	4.4e-02
12	J034429.7+320032	056.1237	+32.0089	0.736	3.2e-02
13	J034435.9+320056	056.1496	+32.0156	1.147	3.7e-02
14	J034436.5+315848	056.1521	+31.9800	2.482	4.9e-02
15	J034454.2+320020	056.2258	+32.0056	0.907	3.4e-02
16	J034459.9+320032	056.2496	+32.0089	1.267	3.9e-02
17	J034507.0+320032	056.2792	+32.0089	0.839	3.3e-02
18	J034358.1+320221	055.9921	+32.0392	0.907	2.6e-02
19	J034358.1+320403	055.9921	+32.0675	4.211	5.7e-02
20	J034448.6+320032	056.2025	+32.0089	2.157	4.4e-02
21	J034516.5+320449	056.3187	+32.0803	1.113	3.6e-02
22	J034520.3+320507	056.3346	+32.0853	1.284	4.2e-02
23	J034050.4+314832	055.2100	+31.8089	0.856	3.3e-02

Table 4—Continued

ID	Name	R.A. (deg)	Decl. (deg)	Mass ( $M_{\odot}$ )	$R_{eff}$ (pc)
24	J034217.5+314620	055.5729	+31.7722	0.325	2.2e-02
25	J034223.1+314550	055.5962	+31.7639	0.308	2.1e-02
26	J034207.1+314720	055.5296	+31.7889	2.088	5.2e-02
NGC 1333					
1	J032925.4+312818	052.3558	+31.4717	0.941	2.8e-02
2	J032918.3+312512	052.3262	+31.4200	7.497	7.2e-02
3	J032907.4+312155	052.2808	+31.3653	5.905	5.1e-02
4	J032914.9+312030	052.3121	+31.3417	2.722	4.9e-02
5	J032859.5+312131	052.2479	+31.3586	7.446	5.3e-02
6	J032901.3+312031	052.2554	+31.3419	15.080	5.9e-02
7	J032835.9+310456	052.1496	+31.0822	1.181	3.6e-02
8	J032832.6+310456	052.1358	+31.0822	1.763	4.2e-02
9	J032842.4+310614	052.1767	+31.1039	2.259	4.3e-02
10	J032847.1+310907	052.1962	+31.1519	0.822	3.2e-02
11	J032829.4+310956	052.1225	+31.1656	1.643	4.5e-02
12	J032831.3+311420	052.1304	+31.2389	0.188	1.6e-02
13	J032836.9+311326	052.1537	+31.2239	3.663	4.8e-02
14	J032926.4+310730	052.3600	+31.1250	0.394	2.2e-02
15	J032923.1+311000	052.3462	+31.1667	0.650	2.9e-02
16	J032919.0+311136	052.3292	+31.1933	3.458	5.4e-02
17	J032910.1+311331	052.2921	+31.2253	24.529	4.5e-02
18	J032855.2+311437	052.2300	+31.2436	12.393	6.2e-02
19	J032908.7+311513	052.2862	+31.2536	8.096	5.5e-02
20	J032906.4+311537	052.2767	+31.2603	6.505	4.1e-02
21	J032908.3+311707	052.2846	+31.2853	2.773	4.2e-02
22	J032906.9+311725	052.2787	+31.2903	1.541	2.7e-02
23	J032852.9+311825	052.2204	+31.3069	0.531	2.6e-02
24	J032855.7+311919	052.2321	+31.3219	0.993	3.2e-02

Table 5. Protostellar Cores in Each Clump

ID	Name	R.A. (deg)	Decl. (deg)	Mass ( $M_{\odot}$ )	$R_{eff}$ pc
B5					
1	03:47:45.3	+32:52:43.4	859.6	776.0	
L1448					
1	J032536.1+304514	051.4004	+30.7539	17.271	5.6e-02
2	J032538.9+304402	051.4121	+30.7339	4.930	3.7e-02
3	J032522.2+304514	051.3425	+30.7539	3.646	3.9e-02
L1455					
1	J032738.3+301353	051.9096	+30.2314	0.496	2.1e-02
2	J032739.2+301259	051.9133	+30.2164	1.968	3.0e-02
3	J032742.9+301228	051.9287	+30.2078	2.105	3.5e-02
4	J032748.0+301210	051.9500	+30.2028	0.531	1.8e-02
B1					
1	J033228.7+310227	053.1196	+31.0408	0.822	3.3e-02
2	J033313.2+311956	053.3050	+31.3322	2.140	4.3e-02
3	J033315.9+310656	053.3162	+31.1156	14.618	6.9e-02
4	J033316.4+310750	053.3183	+31.1306	6.162	5.4e-02
5	J033317.8+310932	053.3242	+31.1589	17.802	8.9e-02
6	J033321.0+310732	053.3375	+31.1256	17.511	6.5e-02
7	J033327.1+310707	053.3629	+31.1186	3.030	5.0e-02
8	J033120.7+304531	052.8362	+30.7586	3.355	4.4e-02
IC 348					
1	J034356.7+320051	055.9862	+32.0142	10.014	5.9e-02
2	J034357.2+320303	055.9883	+32.0508	6.898	4.7e-02
3	J034401.4+320157	056.0058	+32.0325	3.406	4.2e-02
4	J034402.8+320227	056.0117	+32.0408	3.252	3.9e-02
5	J034406.1+320215	056.0254	+32.0375	2.653	4.1e-02
6	J034412.7+320133	056.0529	+32.0258	0.051	8.2e-03
7	J034421.0+315923	056.0875	+31.9897	2.277	5.3e-02
8	J034443.9+320132	056.1829	+32.0256	3.509	4.9e-02
9	J034351.0+320321	055.9625	+32.0558	6.077	5.8e-02
NGC 1333					
1	J032832.2+311108	052.1342	+31.1856	2.003	4.7e-02
2	J032832.6+310044	052.1358	+31.0122	0.496	2.6e-02
3	J032834.5+310702	052.1437	+31.1172	0.359	1.8e-02
4	J032839.2+310556	052.1633	+31.0989	3.132	5.0e-02
5	J032839.3+311826	052.1637	+31.3072	5.820	6.3e-02
6	J032839.8+311750	052.1658	+31.2972	3.560	4.3e-02
7	J032845.2+310549	052.1883	+31.0969	1.352	3.8e-02
8	J032900.3+311201	052.2512	+31.2003	0.753	2.6e-02
9	J032903.6+311455	052.2650	+31.2486	7.497	5.1e-02
10	J032904.6+311843	052.2692	+31.3119	0.633	2.4e-02
11	J032910.2+312143	052.2925	+31.3619	5.580	5.1e-02
12	J032910.7+311824	052.2946	+31.3067	10.818	6.1e-02
13	J032912.0+311306	052.3000	+31.2183	15.200	4.9e-02
14	J032913.4+311354	052.3058	+31.2317	4.605	4.1e-02

Table 5—Continued

ID	Name	R.A. (deg)	Decl. (deg)	Mass ( $M_{\odot}$ )	$R_{eff}$ pc
15	J032917.4+312748	052.3225	+31.4633	3.286	5.5e-02
16	J032918.7+312312	052.3279	+31.3867	1.386	2.9e-02
17	J032919.7+312348	052.3321	+31.3967	3.098	4.6e-02
18	J032951.4+313904	052.4642	+31.6511	1.404	3.3e-02

Table 6. Class 0 in Each Clump

ID	Source	R.A. (J2000)	Decl. (J2000)
L1448			
1	West9	3:25:22.3	30:45:10
2	West25	3:25:35.4	30:45:32
3	West8	3:25:36.2	30:45:17
4	West4	3:25:38.7	30:44:02
L1455			
1	West18	3:27:43.1	30:12:26
B1			
1	West17	3:31:20.6	30:45:29
2	West26	3:32:17.7	30:49:46
3	West50	3:33:14.3	31:07:09
4	West34	3:33:16.2	31:06:51
5	West12	3:33:17.7	31:09:30
6	West41	3:33:21.3	31:07:27
IC 348			
1	East11	3:43:50.6	32:03:24
2	East9	3:43:50.6	32:03:08
3	East4	3:43:56.4	32:00:49
4	East5	3:43:56.6	32:03:03
5	East17	3:44:02.1	32:02:02
NGC 1333			
1	West162	3:28:38.6	31:06:00
2	West33	3:29:00.4	31:11:57
3	West19	3:29:01.8	31:15:34
4	West40	3:29:03.9	31:14:43
5	West87	3:29:06.7	31:15:33
6	West6	3:29:10.3	31:13:28
7	West14	3:29:11.0	31:18:26
8	West13	3:29:11.9	31:13:05
9	West30	3:29:13.5	31:13:54
10	West23	3:29:17.2	31:27:43
11	West37	3:29:18.8	31:23:12
12	West28	3:29:51.7	31:39:03

Table 7. Class I in Each Clump

ID	<i>Spitzer</i> Source Name (JHHMMSS.ss+DDMMSS.s)	c2d classification	R.A. (deg)	Decl. (deg)
B5				
1	J034705.43+324308.5	YSOc_red	56.77262	32.71903
2	J034741.58+325144.1	YSOc	56.92325	32.86225
L1448				
1	J032539.12+304358.2	YSOc_red	51.413	30.73283
2	J032538.83+304406.2	YSOc_red	51.41179	30.73506
3	J032536.22+304515.7	red	51.40092	30.75436
4	J032536.49+304522.2	YSOc_red	51.40204	30.75617
5	J032522.32+304513.9	YSOc_red	51.343	30.75386
L1455				
1	J032800.39+300801.3	YSOc_red	52.00162	30.13369
2	J032738.83+301257.9	YSOc_red	51.91179	30.21608
3	J032739.08+301303.1	YSOc_red	51.91283	30.21753
B1				
1	J033120.98+304530.1	YSOc_red	52.83742	30.75836
2	J033257.84+310608.3	YSOc_red	53.241	31.10231
3	J033309.56+310531.2	YSOc_PAH-em	53.28983	31.092
4	J033313.80+312005.3	YSOc_red	53.3075	31.33481
5	J033316.44+310652.5	red	53.3185	31.11458
6	J033316.65+310755.2	YSOc_red	53.31937	31.132
7	J033320.32+310721.5	YSOc_red	53.33467	31.12264
8	J033327.29+310710.2	YSOc_red	53.36371	31.1195
IC 348				
1	J034329.43+315219.5	YSOc_star+dust(IR1)	55.87262	31.87208
2	J034356.52+320052.8	red	55.9855	32.01467
3	J034356.84+320304.7	YSOc_red	55.98683	32.05131
4	J034402.40+320204.9	YSOc_red	56.01	32.03469
5	J034409.20+320237.8	YSOc_star+dust(IR1)	56.03833	32.04383
6	J034421.35+315932.6	YSOc_red	56.08896	31.99239
7	J034443.32+320131.5	YSOc_red	56.1805	32.02542
8	J034158.67+314821.4	YSOc_red	55.49446	31.80594
9	J034202.17+314802.1	YSOc_red	55.50904	31.80058
NGC 1333				
1	J032832.56+311105.1	YSOc_red	52.13567	31.18475
2	J032834.49+310051.1	YSOc_star+dust(IR1)	52.14371	31.01419
3	J032834.53+310705.5	YSOc	52.14387	31.11819
4	J032837.09+311330.8	YSOc_red	52.15454	31.22522
5	J032839.71+311731.9	YSOc_red	52.16546	31.29219
6	J032840.63+311756.5	red	52.16929	31.29903
7	J032843.28+311732.9	YSOc_star+dust(IR1)	52.18033	31.29247
8	J032845.30+310541.9	YSOc_red	52.18875	31.09497
9	J032851.26+311739.3	YSOc_star+dust(IR2)	52.21358	31.29425
10	J032855.55+311436.7	rising	52.23146	31.24353
11	J032857.36+311415.9	YSOc_red	52.239	31.23775
12	J032858.43+312217.5	YSOc_red	52.24346	31.37153



Table 7—Continued

ID	<i>Spitzer</i> Source Name (JHHMMSS.ss+DDMMSS.s)	c2d classification	R.A. (deg)	Decl. (deg)
13	J032900.55+311200.8	red	52.25229	31.20022
14	J032901.56+312020.6	rising	52.2565	31.33906
15	J032903.33+312314.6	YSOc_red	52.26387	31.38739
16	J032903.78+311603.8	rising	52.26575	31.26772
17	J032904.06+311446.5	YSOc_red	52.26692	31.24625
18	J032907.78+312157.3	rising	52.28242	31.36592
19	J032909.10+312128.7	YSOc	52.28792	31.35797
20	J032910.65+311340.0	YSOc_red	52.29437	31.22778
21	J032910.68+311820.6	YSOc_red	52.2945	31.30572
22	J032910.99+311826.0	YSOc_red	52.29579	31.30722
23	J032911.26+311831.4	YSOc_red	52.29692	31.30872
24	J032912.06+311305.4	YSOc_red	52.30025	31.21817
25	J032912.97+311814.3	YSOc	52.30404	31.30397
26	J032913.54+311358.2	red	52.30642	31.23283
27	J032917.17+312746.5	YSOc_red	52.32154	31.46292
28	J032918.26+312319.9	YSOc_red	52.32608	31.38886
29	J032923.48+313329.5	YSOc_red	52.34783	31.55819
30	J032951.82+313906.0	red	52.46592	31.65167

Table 8. Class Flat in Each Clump

ID	<i>Spitzer</i> Source Name (JHHMMSS.ss+DDMMSS.s)	c2d classification	R.A. (deg)	Decl. (deg)
L1455				
1	J032747.67+301204.5	YSOc_star+dust(IR1)	51.94862	30.20125
2	J032835.03+302009.9	YSOc_star+dust(IR4)	52.14596	30.33608
B1				
1	J033229.17+310240.8	YSOc_star+dust(IR1)	53.12154	31.04467
2	J033306.41+310804.6	YSOc_star+dust(IR1)	53.27671	31.13461
3	J033312.84+312124.2	YSOc_star+dust(IR1)	53.3035	31.35672
IC 348				
1	J034256.05+315644.8	YSOc	55.73354	31.94578
2	J034336.02+315009.0	YSOc_star+dust(IR1)	55.90008	31.83583
3	J034345.17+320358.6	YSOc_star+dust(IR1)	55.93821	32.06628
4	J034359.41+320035.7	YSOc_red	55.99754	32.00992
5	J034412.98+320135.5	YSOc	56.05408	32.02653
6	J034435.34+322837.2	YSOc_red	56.14725	32.477
7	J034141.09+314804.6	YSOc	55.42121	31.80128
NGC 1333				
1	J032838.78+311806.6	YSOc_star+dust(IR2)	52.16158	31.30183
2	J032848.77+311608.8	YSOc_red	52.20321	31.26911
3	J032856.60+310737.0	YSOc_red	52.23583	31.12694
4	J032858.26+312209.2	YSOc_star+dust(IR2)	52.24275	31.36922
5	J032859.23+312032.5	YSOc_star+dust(IR1)	52.24679	31.34236
6	J032859.32+311548.7	YSOc_star+dust(IR4)	52.24717	31.26353
7	J032901.88+311653.2	YSOc_star+dust(IR2)	52.25783	31.28144
8	J032904.95+312038.4	YSOc_star+dust(IR2)	52.27062	31.344
9	J032911.89+312127.0	YSOc	52.29954	31.3575
10	J032912.06+311301.7	YSOc_red	52.30025	31.21714
11	J032918.67+312017.7	YSOc_star+dust(IR2)	52.32779	31.33825
12	J032920.06+312407.5	YSOc_star+dust(IR2)	52.33358	31.40208
13	J032920.44+311834.2	YSOc_star+dust(IR1)	52.33517	31.3095
14	J032924.09+311957.6	YSOc_star+dust(IR2)	52.35037	31.33267

Table 9. Class II in Each Clump

ID	<i>Spitzer</i> Source Name (JHHMMSS.ss+DDMMSS.s)	c2d classification	R.A. (deg)	Decl. (deg)
L1455				
1	J032738.25+301358.6	YSOc_star+dust(IR4)	51.90937	30.23294
2	J032800.09+300847.0	YSOc_star+dust(IR2)	52.00037	30.14639
B1				
1	J033232.99+310221.7	YSOc_star+dust(IR1)	53.13746	31.03936
2	J033234.05+310055.8	YSOc_star+dust(IR2)	53.14187	31.0155
3	J033247.20+305916.3	YSOc_star+dust(IR2)	53.19667	30.98786
4	J033330.41+311050.6	YSOc_star+dust(IR1)	53.37671	31.18072
5	J033341.29+311341.0	YSOc_star+dust(IR1)	53.42204	31.22806
IC 348				
1	J034244.50+315958.7	YSOc_star+dust(IR1)	55.68542	31.99964
2	J034249.18+315011.2	YSOc_star+dust(IR4)	55.70492	31.83644
3	J034255.95+315842.0	YSOc_star+dust(IR1)	55.73312	31.97833
4	J034313.70+320045.2	YSOc_star+dust(IR2)	55.80708	32.01256
5	J034325.48+315516.5	YSOc_star+dust(MP1)	55.85617	31.92125
6	J034328.21+320159.1	YSOc_star+dust(IR2)	55.86754	32.03308
7	J034355.00+320103.1	YSOc_star+dust(IR2)	55.97917	32.01753
8	J034355.24+315532.1	YSOc_star+dust(IR1)	55.98017	31.92558
9	J034356.03+320213.3	YSOc_star+dust(IR2)	55.98346	32.03703
10	J034357.23+320133.7	YSOc_star+dust(IR2)	55.98846	32.02603
11	J034359.65+320154.1	YSOc	55.99854	32.03169
12	J034400.48+320432.7	YSOc_red	56.002	32.07575
13	J034405.78+320001.1	YSOc_star+dust(IR1)	56.02408	32.00031
14	J034405.78+320028.5	YSOc	56.02408	32.00792
15	J034410.13+320404.5	YSOc_star+dust(IR2)	56.04221	32.06792
16	J034411.63+320313.1	YSOc_star+dust(IR3)	56.04846	32.05364
17	J034415.84+315936.7	YSOc_star+dust(IR2)	56.066	31.99353
18	J034418.17+320457.0	YSOc_star+dust(IR3)	56.07571	32.0825
19	J034419.25+320734.7	YSOc_star+dust(IR4)	56.08021	32.12631
20	J034420.18+320856.5	YSOc_star+dust(IR2)	56.08408	32.14903
21	J034421.23+320114.5	YSOc_star+dust(IR4)	56.08846	32.02069
22	J034422.29+320542.8	YSOc_star+dust(IR3)	56.09287	32.09522
23	J034422.58+320153.6	YSOc_star+dust(IR4)	56.09408	32.03156
24	J034424.46+320143.7	YSOc_star+dust(IR2)	56.10192	32.02881
25	J034425.55+320617.1	YSOc_star+dust(IR4)	56.10646	32.10475
26	J034426.04+320430.4	YSOc_star+dust(IR1)	56.1085	32.07511
27	J034426.70+320820.3	YSOc_star+dust(IR2)	56.11125	32.13897
28	J034428.51+315954.0	YSOc_star+dust(IR3)	56.11879	31.99833
29	J034428.95+320137.9	YSOc_star+dust(IR2)	56.12062	32.02719
30	J034429.80+320054.6	YSOc_star+dust(IR2)	56.12417	32.01517
31	J034431.19+320558.9	YSOc_star+dust(IR4)	56.12996	32.09969
32	J034431.37+320014.2	YSOc_star+dust(IR2)	56.13071	32.00394
33	J034433.79+315830.2	YSOc_star+dust(IR4)	56.14079	31.97506
34	J034434.81+315655.2	YSOc_star+dust(IR4)	56.14504	31.94867
35	J034445.20+320119.6	YSOc_star+dust(IR1)	56.18833	32.02211

Table 9—Continued

ID	<i>Spitzer</i> Source Name (JHHMMSS.ss+DDMMSS.s)	c2d classification	R.A. (deg)	Decl. (deg)
36	J034124.42+315327.9	YSOc_star+dust(IR1)	55.35175	31.89108
37	J034153.26+315019.2	YSOc_star+dust(IR1)	55.47192	31.83867
38	J034201.01+314913.4	YSOc_star+dust(IR3)	55.50421	31.82039
39	J034204.34+314711.6	YSOc_star+dust(IR1)	55.51808	31.78656
40	J034210.69+314705.6	YSOc_star+dust(IR3)	55.54454	31.78489
41	J034301.94+314435.6	YSOc_star+dust(IR1)	55.75808	31.74322
42	J034321.47+314246.3	YSOc_star+dust(IR3)	55.83946	31.71286
NGC 1333				
1	J032844.09+312052.7	YSOc_star+dust(IR2)	52.18371	31.34797
2	J032847.65+312406.0	YSOc_star+dust(IR1)	52.19854	31.40167
3	J032847.84+311655.1	YSOc_star+dust(IR2)	52.19933	31.28197
4	J032851.03+311818.5	YSOc_star+dust(IR2)	52.21262	31.30514
5	J032851.08+311632.4	YSOc_star+dust(IR2)	52.21283	31.27567
6	J032851.20+311954.8	YSOc_star+dust(IR2)	52.21333	31.33189
7	J032852.15+311547.1	YSOc_star+dust(IR2)	52.21729	31.26308
8	J032852.17+312245.3	YSOc_star+dust(IR3)	52.21737	31.37925
9	J032852.92+311626.4	YSOc_star+dust(IR2)	52.2205	31.274
10	J032853.96+311809.3	YSOc_star+dust(IR3)	52.22483	31.30258
11	J032854.09+311654.2	YSOc_star+dust(IR3)	52.22537	31.28172
12	J032854.63+311651.1	YSOc_star+dust(IR2)	52.22762	31.28086
13	J032855.08+311628.7	YSOc_star+dust(IR1)	52.2295	31.27464
14	J032856.12+311908.4	YSOc	52.23383	31.319
15	J032856.32+312227.9	YSOc_star+dust(IR2)	52.23467	31.37442
16	J032856.65+311835.5	YSOc_star+dust(IR2)	52.23604	31.30986
17	J032856.97+311622.3	YSOc_star+dust(IR4)	52.23737	31.27286
18	J032857.18+311534.6	YSOc_star+dust(IR2)	52.23825	31.25961
19	J032858.27+312202.0	YSOc_star+dust(IR1)	52.24279	31.36722
20	J032859.56+312146.7	YSOc_star+dust(IR1)	52.24817	31.36297
21	J032902.81+312217.2	YSOc_star+dust(IR2)	52.26171	31.37144
22	J032903.15+312238.0	YSOc_star+dust(IR1)	52.26312	31.37722
23	J032903.22+312545.1	YSOc_star+dust(IR2)	52.26342	31.42919
24	J032903.87+312148.6	YSOc_star+dust(IR1)	52.26612	31.3635
25	J032904.68+311659.0	YSOc	52.2695	31.28306
26	J032904.73+311134.9	YSOc	52.26971	31.19303
27	J032905.18+312036.9	YSOc_red	52.27158	31.34358
28	J032906.33+311346.4	YSOc_star+dust(IR3)	52.27637	31.22956
29	J032907.96+312251.4	YSOc_star+dust(IR2)	52.28317	31.38094
30	J032909.34+312104.1	YSOc_star+dust(IR3)	52.28892	31.35114
31	J032909.40+311413.8	YSOc	52.28917	31.23717
32	J032909.49+312720.9	YSOc_star+dust(IR2)	52.28954	31.45581
33	J032909.65+312256.3	YSOc_star+dust(IR4)	52.29021	31.38231
34	J032910.47+312334.7	YSOc_star+dust(IR2)	52.29362	31.39297
35	J032910.84+311642.6	YSOc_star+dust(IR1)	52.29517	31.2785
36	J032913.14+312252.8	YSOc_star+dust(IR2)	52.30475	31.38133
37	J032914.40+311444.1	YSOc	52.31	31.24558

Table 9—Continued

ID	<i>Spitzer</i> Source Name (JHHMMSS.ss+DDMMSS.s)	c2d classification	R.A. (deg)	Decl. (deg)
38	J032916.61+312349.4	YSOc_star+dust(IR2)	52.31921	31.39706
39	J032916.83+312325.1	YSOc_star+dust(IR2)	52.32012	31.39031
40	J032917.68+312245.0	YSOc_star+dust(IR1)	52.32367	31.37917
41	J032917.78+311948.0	YSOc_star+dust(IR2)	52.32408	31.33
42	J032918.74+312325.4	YSOc_star+dust(IR2)	52.32808	31.39039
43	J032921.57+312110.3	YSOc_star+dust(IR2)	52.33987	31.35286
44	J032921.87+311536.2	YSOc_star+dust(IR2)	52.34112	31.26006
45	J032923.17+312030.2	YSOc_star+dust(IR2)	52.34654	31.34172
46	J032923.25+312653.1	YSOc_star+dust(IR2)	52.34687	31.44808
47	J032925.93+312640.1	YSOc	52.35804	31.44447
48	J032929.27+311834.7	YSOc_star+dust(IR4)	52.37196	31.30964
49	J032929.80+312102.6	YSOc_star+dust(IR3)	52.37417	31.35072
50	J032930.40+311903.3	YSOc_star+dust(IR2)	52.37667	31.31758
51	J032932.57+312436.9	YSOc_star+dust(IR1)	52.38571	31.41025
52	J032932.88+312712.6	YSOc_star+dust(IR2)	52.387	31.4535
53	J032937.73+312202.5	YSOc_star+dust(IR2)	52.40721	31.36736

Table 10. Class III in Each Clump

ID	<i>Spitzer</i> Source Name (JHHMMSS.ss+DDMMSS.s)	c2d classification	R.A. (deg)	Decl. (deg)
IC 348				
1	J034409.16+320709.3	YSOc_star+dust(MP1)	56.03817	32.11925
2	J034430.14+320118.2	YSOc_star+dust(IR4)	56.12558	32.02172
3	J034223.33+315742.7	YSOc_star+dust(IR4)	55.59721	31.96186
4	J034436.96+320645.2	YSOc_star+dust(IR4)	56.154	32.11256
NGC 1333				
1	J032843.24+311042.7	YSOc_star+dust(IR4)	52.18017	31.17853
2	J032857.21+311419.1	YSOc_star+dust(MP1)	52.23837	31.23864
3	J032858.11+311803.7	YSOc_star+dust(MP1)	52.24212	31.30103
4	J032916.69+311618.2	YSOc_star+dust(MP1)	52.31954	31.27172
5	J032926.81+312647.6	YSOc_star+dust(MP1)	52.36171	31.44656